Optics and Lasers in Engineering 170 (2023) 107763

Contents lists available at ScienceDirect

Optics and Lasers in Engineering

journal homepage: www.elsevier.com/locate/optlaseng

A liquid crystal optical sensor for simple and quantitative determination of dimethyl methylphosphonate using laser speckle

Yuxiang Yan [a,b], Ning Bu [a,b], Xiaoquan Bai [a,b], Mei Wang [a,b], Yifei Ma [a,b], Suotang Jia [a,b], Xuyuan Chen [a,b,c], Zhaomin Tong [a,b,*]

[a] State Key Laboratory of Quantum Optics and Quantum Optics Devices, Institute of Laser Spectroscopy, Shanxi University, Taiyuan, 030006, China
[b] Collaborative Innovation Center of Extreme Optics, Shanxi University, Taiyuan, 030006, China
[c] Faculty of Technology, Natural Sciences and Maritime Sciences, Department of Microsystems, University of South-Eastern Norway, Borre, N-3184, Norway

ARTICLE INFO

Keywords:
Liquid crystal
Laser speckle
Correlation coefficient
Organophosphorus vapor
4-cyano-4′-pentylbiphenyl

ABSTRACT [1]

A new method is reported for determining the concentration of dimethyl methylphosphonate (DMMP) vapor based on the capture of laser speckles from a liquid crystal (LC) sensor. The sensor comprises a film of the nematic LC, 4-cyano-4′-pentylbiphenyl, anchored to a carboxy-terminated self-assembled monolayer of 11-mercaptoundecanoic acid via interaction with copper ions. A linearly polarized laser beam is transmitted through the sensor and irradiated onto a rough diffuser. A charge-coupled device camera is used to capture speckle images from the LC sensor and calculate the correlation coefficient. DMMP vapor is selectively detected over a 500 ppb to 5 ppm concentration range, demonstrating the feasibility of the method for determining vapor phase concentrations of organophosphorus compounds. Compared with previous methods that use a polarizing optical microscope to image the LC film, our approach does not require complex instrumentation and reduces the size, complexity, and cost of the detection system. The detection methodology described in this study provides new ideas for LC-based sensing of organophosphorus vapors.

1. Introduction

Organophosphorus compounds (OPs) are a class of toxic organic molecules, such as Sarin, that are commonly used as chemical warfare agents [1]. These dangerous substances can cause irreversible physiological damage within seconds or death within a few minutes after exposure [2,3] The use of OP pesticides in agriculture also has considerably increased [4]. Although OP pesticides are not as toxic as chemical warfare agents, they still pose a threat to the environment and human health. Thus, there is a need to develop sensors for the detection of organophosphorus compounds.

Methods for detecting OPs include gas chromatography [5] and ion mobility spectroscopy [6], which can identify and quantify analytes based on their chemical composition and can function in complex environments. However, these methodologies require complex instrumentation, which is expensive and lacks portability. Many studies have addressed these issues while undertaking the detection of OPs. For example, surface acoustic wave spectroscopy employs a sensitive surface film placed between two transducers. The film selectively adsorbs the target gas, which alters the surface acoustic wave propagation velocity and causes corresponding changes in the frequency or phase of the transducer signal [7,8]. The quartz crystal microbalance [9,10] and electrochemical techniques based on carbon nanotubes [11] also have been used to detect OPs. The above techniques reduce cost and improve portability to some extent. However, the methods are susceptible to humidity and to false positives due to the presence of other gases. Thus, a need exists for a detection technology that is sensitive and selective, but is simple, portable, inexpensive, and power-independent.

Liquid crystals (LCs) have attracted recent attention due to their unique optical properties and response to stimuli. For example, Devi et al. reported LC-based sensors for detecting biomolecules and heavy-metal ions [12–14]. Many studies have also confirmed that LCs can be used in the detection of OPs. LC-based detection involves the use of specific metal cations to affix the liquid crystal within a LC film. When OPs present, the ability of metal cations to anchor the LCs is weakened because metal cations prefer binding to OPs instead of LCs, which results

* Corresponding author.
E-mail address: zhaomin.tong@sxu.edu.cn (Z. Tong).

[1] dimethyl methylphosphonate (DMMP); liquid crystal (LC); 4-cyano-4′-pentylbiphenyl (5CB); self-assembled monolayer (SAM); 11-mercaptoundecanoic acid (MUA); charge-coupled device (CCD); organophosphorus compounds (OPs); transmission electron microscopy (TEM);

https://doi.org/10.1016/j.optlaseng.2023.107763
Received 4 February 2023; Received in revised form 22 April 2023; Accepted 25 July 2023

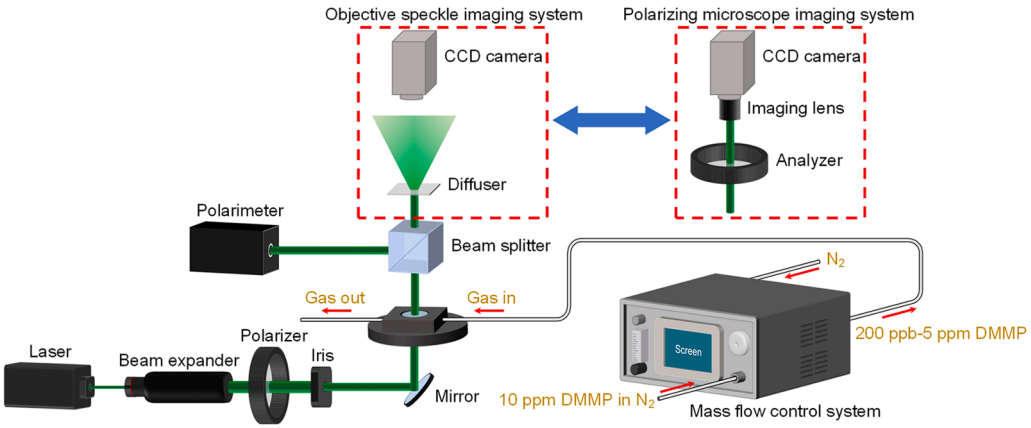

Fig. 1. Schematic illustration of the detection system. The left and right dashed boxes indicate the detection method used in this work and in previous studies, respectively.

in the change of the optical properties of the LC film. For example, Sridharamurthy et al. reported a LC sensor capable of responding to 10 ppm dimethyl methylphosphonate (DMMP) vapor. The sensor was fabricated by forming a self-assembled monolayer (SAM) of 11-mercaptoundecanoic acid (MUA) on a thin, evaporated gold film covering an array of micropillars. The surface was functionalized with copper perchlorate, and 4-cyano-4′-pentylbiphenyl (5CB) was introduced to the film [15]. The microstructure used the capillary force generated by the micropillar array to support the LC film. Bungabong et al. reported a method using 5CB doped with 0.05−50 mM copper perchlorate as an optical sensor to detect DMMP vapor [16]. Copper-doped 5CB was filled into a copper transmission electron microscopy (TEM) grid, which was placed on the surface of a glass slide and monitored as the orientation of 5CB gradually changed from planar to homeotropic. This LC sensor was easily fabricated and afforded a 3 ppb detection limit, which was lower than that of previous studies. However, the preparation time was long (1–31 days), and the recovery response of the sensor was poor. Abbott and co-workers used obliquely deposited gold surfaces covered with SAMs to capture metal ions. Liquid crystals based on 5CB, 4-cyano-4-′-octylbiphenyl (8CB), or the liquid crystal mixture E7, supported on chemical surfaces have been used to detect OPs [17–19]. A variety of procedures have been used to prepare LC films. Methods include spin coating onto functionalized glass slides and filling TEM grids, fabricated microwells, or fabricated micropillars with LCs [19–21]. These techniques typically use a polarizing optical microscope to observe and calculate the change in luminosity after light transmission through the LC film to establish the concentration of the detected gas. Moreover, the detection systems are bulky, expensive, and complicated to operate and often fail to accurately determine the target gas concentration.

The high toxicity of chemical warfare agents and organophosphorus pesticides presents a danger for use in experimental research. Therefore, we employ DMMP as a simulation compound, because it is similar to Sarin in terms of structure, functional groups, and properties while conveying low toxicity [22,23]. We report a new method for the detection of DMMP vapor based on LC sensors constructed by forming LC films on the chemically functionalized surfaces of glass slides. The fabricated sensor is placed in a chamber and linearly polarized laser is transmitted through the LC film and irradiated on a rough diffuser. A charge-coupled device (CCD) camera without a mounted imaging lens is placed above the diffuser to capture speckle images in real time. We passed DMMP vapors at different concentrations, several organic vapors, and pure nitrogen at different relative humidity into the chamber, and established the concentration range, detection limit, and selectivity of DMMP by calculating the correlation coefficients of the speckle images.

2. Experimental section

2.1. Materials

11-Mercaptoundecanoic acid (MUA) and anhydrous ethanol were purchased from Aladdin Biochemistry Technology Co., Ltd. (Shanghai, China). Copper(II) perchlorate hexahydrate was purchased from Sigma–Aldrich (Singapore). 5CB was purchased from Instec, Inc. Titanium (99.999%) and gold (99.999%) were purchased from Advanced Materials (Spring Valley, NY). DMMP in nitrogen at a nominal concentration of 10 ppm was purchased from Dalian Special Gases Co., Ltd. (Dalian, China). All chemicals and solvents were of analytical reagent grade and were used as received without further purification.

2.2. Deposition of gold films

Semi-transparent 200-Å gold films were deposited onto cleaned glass slides mounted on a fixed holder within an electron beam evaporator (Ei-5z, ULVAC). A 100-Å titanium layer was first deposited on the glass slides to promote adhesion of the gold film. The rates of gold and titanium deposition were 0.2 Å/s. The pressure in the evaporator was maintained at $<5 \times 10^{-4}$ Pa before and during deposition. The procedure for gold film deposition was based on published methods with slight modifications [24].

2.3. Preparation of functionalized gold surfaces

The protocol for preparing functionalized gold surfaces was slightly modified from a procedure published in literature [24]. MUA SAMs were prepared by overnight immersion of gold-coated glass slides in a 2 mM MUA solution in ethanol. The SAMs were rinsed copiously with ethanol and dried under a nitrogen stream. Copper ions (Cu^{2+}) were immediately deposited onto the carboxylate SAMs by dip-coating from ethanolic solutions of copper perchlorate (with concentrations of 10, 5, 1, 0.5 mM) at a withdrawal speed of 300 μm/s.

2.4. Formation of thin LC films

After dip-coating Cu^{2+} onto the SAMs, a 20-μm thick copper TEM grid (Zhongjingkeyi Technology Co., Ltd, Beijing, China) with 50 mesh was placed on top of the surface. The TEM grids were filled with 5CB using a capillary cube, and excess 5CB was removed with an empty capillary cube.

2.5. Detection system and sensor exposure to DMMP

The details of the detection system are shown in Fig. 1. A 0.7-mm

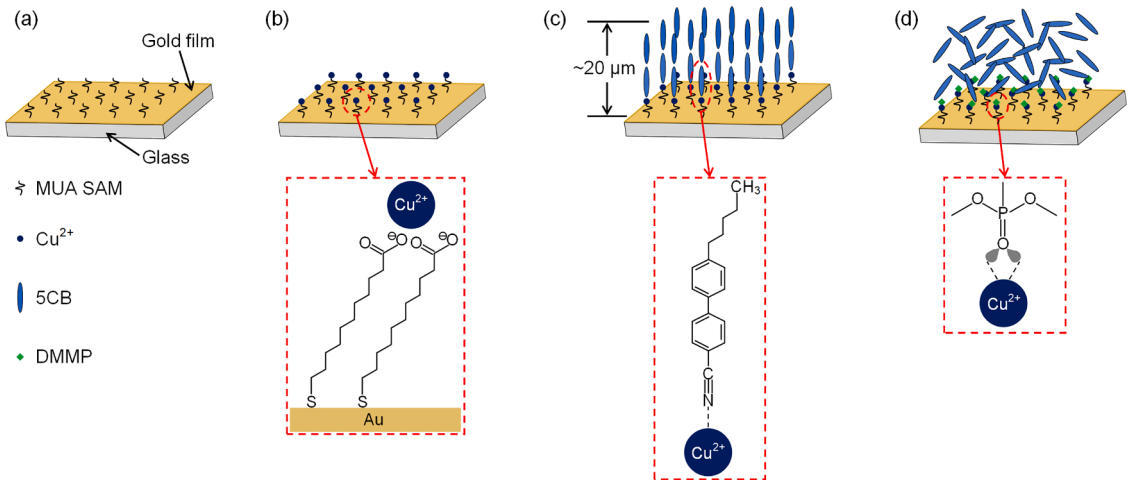

Fig. 2. Schematic of the stepwise assembly of a LC film and principle of DMMP detection. (a) Formation of MUA SAMs on a gold-coated surface. (b) Deposition of Cu^{2+} onto MUA SAMs by dip-coating. (c) Formation of a homeotropically orientated LC film. (d) Structural transition within the LC film upon complexation of Cu^{2+} by DMMP and displacement of the 5CB nitrile group.

diameter beam of highly coherent laser was emitted from a solid-state laser (LCX-532S-100-CSB-PPF, Oxxius). The beam diameter was enlarged to 7 mm by a beam expander. The expanded beam was passed through a linear polarizer whose polarization axis was perpendicular to the horizontal. The beam aperture was redefined by an iris of ~3 mm diameter. The redefined laser beam was reflected by a mirror into a chamber containing the LC sensor with an incident window below and an exit window above the sensor. Glass sheets on the incident and exit windows facilitated transmission of the polarized light through the sensor. The exiting beam was divided by a 50:50 beam splitter, with one beam directed to a polarimeter (PMI-VIS, Meadowlark Optics) to record the polarization state, and the other beam directed to a rough diffuser to form speckles. A CCD camera without a mounted imaging lens was placed above the diffuser to capture the speckle images. The rough diffuser and CCD camera comprised the speckle imaging system. Polarizing microscopic imaging systems used in previous studies comprise crossed polarizers (a polarizer and an analyzer) and a CCD camera with a mounted imaging lens and usually include an optical zooming module between the chamber and analyzer [16,21,24].

The inlet of the sample chamber was connected to a mass flow control system (MF-3D, Zhongji), which modulated the DMMP vapor concentration by dilution with nitrogen gas. DMMP concentrations in this study ranged from 200 ppb to 5 ppm at a constant flow rate of 200 mL/min.

3. Results and discussion

3.1. Gas detection principle

The SAMs were formed by attachment of MUA to the gold surface via sulfhydryl−Au bonding (Fig. 2a). The surface was functionalized by complexing Cu^{2+} to the carboxylate groups of MUA (Cu^{2+}-MUA, Fig. 2b). A TEM grid was then placed on the surface and filled with 5CB. The nitrile group (—CN) of 5CB forms a weak complex with the surface-immobilized Cu^{2+} creating the homeotropic anchoring (parallel to the surface normal) of 5CB at the 5CB-Cu^{2+} interface. Previous studies have established that surface-induced orientations of LCs can be communicated by as much as ~100 μm from the interface into the bulk of a liquid crystalline phase. Thus, the LCs assume a homeotropic orientation at their air-LC or N_2-LC interfaces resulting in a homeotropic alignment of 5CB throughout the LC film (Fig. 2c) [25]. Copper(II) has a greater affinity for the phosphoryl group of DMMP than for the nitrile group of 5CB. Thus, when DMMP molecules diffuse through the LC film to the 5CB-Cu^{2+} interface, 5CB is competitively displaced from its complex with Cu^{2+} and the homeotropic orientation of the LC film is disrupted. The altered alignment of 5CB within the film changes the polarization state of the transmitted laser beam (Fig. 2d) [26].

3.2. Speckle measurement mechanism

When a highly coherent laser beam illuminates a rough surface, bright and dark distributions of grainy light (termed ``speckles'') are formed [27]. Goodman has demonstrated that different laser polarization states result in different speckle patterns [28]. Tong et al. have shown that when the direction of polarized laser is rotated, the correlation coefficient between the speckle patterns formed before and after rotation varies as the square of the cosine function [29]. Owing to the birefringence properties of homeotropically oriented 5CB in the LC films before exposure to DMMP, the polarization state of the laser does not change when the laser is transmitted through the film. After exposure to DMMP, the loss of 5CB attachment at the bottom of the film triggers a transition from a homeotropic to a planar or tilted orientation (Fig. 2c, d). This transformation alters the polarization state of the laser beam. Concurrently, laser transmitted to the rough diffuser forms speckles, which are captured in real time by a CCD camera (PL-B781, Edmund Optics) without a mounted imaging lens. Individual speckle images were taken at 10 s intervals.

The correlation coefficient, $\rho_{m,n}$, between the mth and nth speckle images is defined as the ratio between the covariance of I_m and I_n and the product of their standard deviations,

$$\rho_{m,n} = \frac{\mathrm{cov}(I_m, I_n)}{\sigma_m \sigma_n}, \tag{1}$$

where I_m, I_n, σ_m, and σ_n are the mth and nth speckle intensities and the standard deviations of the speckle images, respectively. Using the equations for the speckle correlation coefficient in [28,29], the correlation coefficient, $\rho_{m,n}$, between the mth and nth speckle images is calculated as

$$\rho_{m,n} = \frac{\overline{(I_m - \overline{I_m})(I_n - \overline{I_n})}}{\sigma_m \sigma_n}, \tag{2}$$

where $\overline{I}_m$ and $\overline{I}_n$ are the mean values of the mth and nth speckle intensities, respectively. Each speckle image with 792 × 600 pixels is read as a separate array using MATLAB. The correlation coefficients between all captured speckle images and the first captured speckle image (i.e., $m = 1$ and $n = 1, 2, \ldots, N$, where N is the number of all speckle images) were calculated from these results.

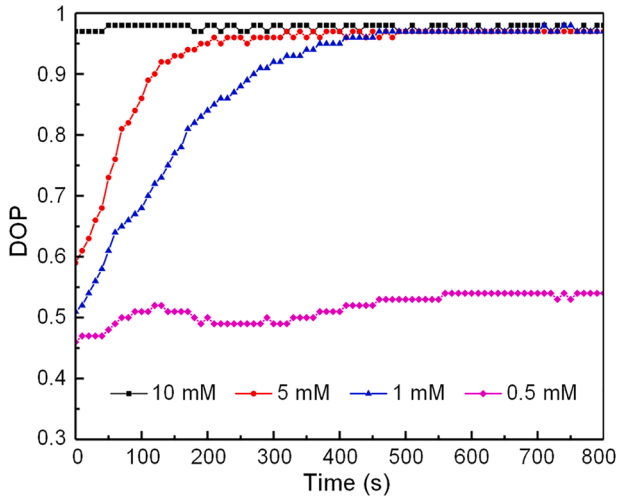

Fig. 3. Change in the DOP of laser transmitted through 5CB-Cu^{2+} LC films.

3.3. Effects of Cu^{2+} concentration on LC alignment

0.5, 1, 5, and 10 mM Cu^{2+} solutions in ethanol were obtained by serial dilution of a 50 mM copper(II) stock solution prepared from copper perchlorate. MUA SAMs on gold-coated glass slides were functionalized by dip-coating in the above solutions at a withdrawal speed of 300 μm/s. LC films of a prescribed thickness were fashioned on the functionalized surfaces by filling 5CB into TEM grids. Previous studies have reported that capillary force firmly holds LCs within microwell and micropillar arrays after filling. Thus, stable films are formed that are resistant to gravity (tilting of the device) and shock [21].

A previous work has also established that LC molecules within the film prepared by filling TEM grids with 5CB gradually establish a homeotropic alignment due to coordination interactions between the —CN group of 5CB and Cu^{2+} [26]. The refractive index of 5CB under incident light equals its normal value, n_o, when the LC is in a homeotropic orientation. Thus, when linearly polarized laser is transmitted through the LC film, the difference in refractive index, Δn, between the horizontal and vertical polarization components, which are perpendicular to the direction of propagation direction, is zero (i.e., $\Delta n = n_o - n_o = 0$). This result means that the phase difference between the orthogonal polarization components of the transmitted laser beam is also 0, which confirms that the polarization state of the transmitted laser beam is unchanged upon passage through the LC film.

A polarimeter was used to determine the polarization state of the incident light by use of the Stokes parameters. We used the degree of polarization (DOP) to characterize the impact of the Cu^{2+} concentration on the homeotropic orientation of 5CB. The DOP describes the percentage of an electromagnetic wave that is polarized and is defined as the fraction of the total power that is carried by the polarized component. DOP is calculated using the Stokes parameters S_0, S_1, S_2, and S_3 [30],

$$DOP = \frac{\sqrt{S_1^2 + S_2^2 + S_3^2}}{S_0}, \tag{3}$$

where S_0 is the total light intensity, and S_1, S_2 and S_3 are the intensity differences between the horizontal and vertical linearly polarized components, the +45° and −45° linearly polarized components, and the right and left circularly polarized components, respectively. The DOP of fully polarized light is 1, whereas that of unpolarized light is 0. DOP values between 0 and 1 correspond to partially polarized waves.

The DOP of linearly polarized laser that is not transmitted through the LC film is unity. Previous work has demonstrated that, if random changes occur in phase retardation at local areas within a LC cell or in the angle of polarization of linearly polarized light, the DOP of the transmitted light decreases [31,32]. At the initial stage of 5CB filling in a TEM grid, the LC is not coordinated by Cu^{2+} and does not adopt a homeotropic orientation. 5CB orientation is random in many areas of the film, and the linearly polarized laser has random phase retardation and reduces the DOP of the transmitted beam. Figure 3 shows the time dependence of DOP for laser transmitted through several 5CB-Cu^{2+} films. Surfaces functionalized with 10, 5, and 1 mM solutions of Cu^{2+} in ethanol exhibit a stable DOP ≈ 1, which is indicative of nearly complete transformation to a homeotropic orientation, at $t = 100$, 250, and 550 s, respectively. DOP at $t = 800$ s equals 0.98, 0.96, and 0.97, respectively, for the above films. However, when a film is functionalized with 0.5 mM Cu^{2+}, DOP increases only to 0.54 at $t = 800$ s. Thus, the 5CB in this film does not achieve a homeotropic orientation. We conclude that the time required for 5CB to achieve homeotropic orientation depends on the Cu^{2+} concentration and that this time increases with decreasing copper concentration, apart from the failure to achieve complete homeotropic orientation with 0.5 mM Cu^{2+}. We also note that the DOP of the transmitted laser does not exactly equal unity and speculate that this result may be due to 5CB disordering near the edges of the TEM grids [33].

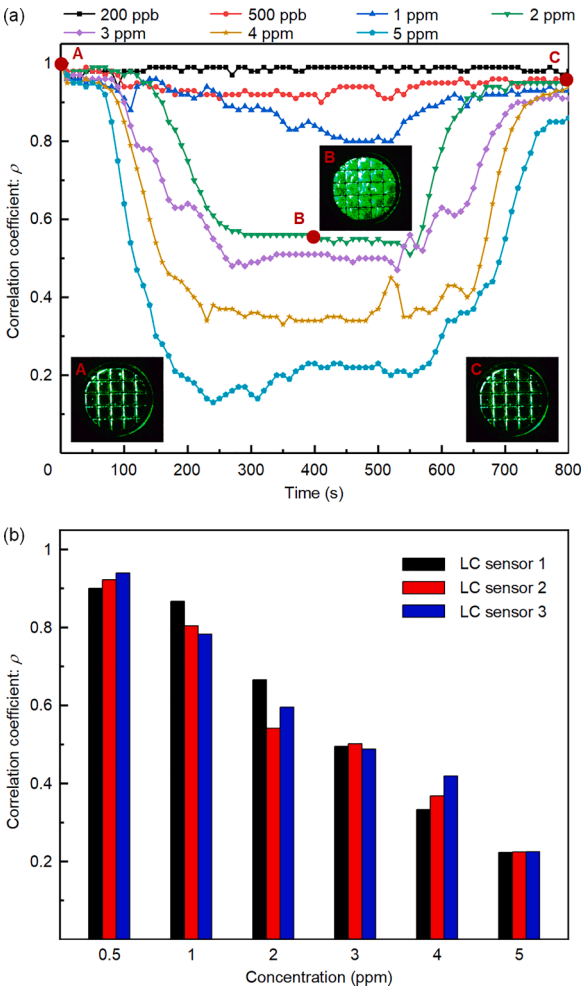

Fig. 4. (a) Time-dependent changes in the correlation coefficient of laser transmitted through LC films on Cu^{2+}-MUA SAMs following exposure to various concentrations of DMMP. Images of the LC film between crossed polarizers are shown at points A, B, and C. (b) Repeatability measurement of three sensors exposed to DMMP vapor for 500 s.

3.4. Gas sensor response and reversibility

We studied the response of 5CB films to gaseous streams containing

different concentrations of DMMP vapor and investigated the relationship between DMMP concentration and correlation coefficient. We also investigated the reversibility of the 5CB-film response upon contact with gaseous streams containing DMMP followed by exposure to pure nitrogen. Previous work has shown that the interaction between DMMP and metal ions (Cu^{2+} or Al^{3+}) in these films is a reversible equilibrium rather than an irreversible chemical transformation [34].

An earlier study found that the detection limit of the DMMP sensor decreased with decreasing Cu^{2+} concentration based on the assumption that the 5CB was homeotropically oriented [16]. Thus, we functionalized gold-coated glass slides with 1 mM ethanol solutions of copper perchlorate and prepared LC films on the chemically functionalized surfaces. DMMP vapor at concentrations of 200 ppb to 5 ppm, obtained by diluting 10 ppm DMMP using the mass flow control system, were passed into the detection chamber. Figure 4(a) shows the change in correlation coefficient as different DMMP vapor concentrations are passed into the chamber at 200 mL/min. The correlation coefficient does not decrease significantly for the sample exposed to 200 ppb DMMP for 500 s. However, the correlation coefficient decreases with time at all concentrations upon exposure to vapors containing ≥500 ppb DMMP and then gradually increases when the flow of DMMP vapor is stopped and the sample is exposed to a pure nitrogen stream for 300 s.

When DMMP vapor flows into the detection chamber, a concentration gradient is established between the LC film and the gaseous stream. DMMP gradually diffuses into the LC film along this gradient and forms a Cu^{2+}-DMMP complex at the bottom of the film. This interaction removes the point of 5CB attachment within the film and precipitates a transition from a homeotropic orientation to a planar or tilted one [34]. When linearly polarized laser is transmitted through the film, the birefringence properties of 5CB lead to non-zero differences in refractive index and phase between the orthogonal polarization components. This change alters the polarization state of the transmitted laser beam. When the surface coverage of coordinated DMMP molecules exceeds a threshold value, liquid crystals at the LC-substrate interface become aligned parallel to or tilted with respect to the surface plane [34]. When the film is exposed to 200 ppb DMMP vapor for 500 s, the correlation coefficient scarcely changes from its initial value of 1 to 0.99 (Fig. 4(a)). Thus, the DMMP coverage at the LC-substrate interface did not exceed the threshold value. The small changes in correlation coefficient observed for this sample may be the result of small alterations in 5CB orientation at the TEM grid edges or unavoidable mechanical vibrations. At ≥500 ppb DMMP vapor concentrations, the correlation coefficient decreases with time at all concentrations and the rate of response increases with increasing DMMP concentration. We therefor associate changes in the correlation coefficient and rate of response to changes in the DMMP vapor concentration. Greater DMMP concentrations lead to larger concentration gradients, enhanced diffusion of DMMP into the LC film, faster diffusion rates, and more extensive displacement of Cu^{2+} from 5CB. When equilibrium is achieved on both sides of the interface, the correlation coefficient stabilizes at a characteristic value. When pure nitrogen gas is directed into the chamber, DMMP diffuses out of the LC film and is expelled from the chamber. 5CB now reattaches to Cu^{2+}, and its return to a homeotropic alignment causes the correlation coefficient to gradually increase. However, the correlation coefficient does not return to its initial value of $\rho = 1$ when pure nitrogen is passed through the chamber for 300 s. For example, exposure to 5 ppm DMMP vapor followed by exposure to pure nitrogen leads only to $\rho = 0.85$ at $t = 800$ s (Fig. 4(a)). We believe that this behavior is caused by metal salts that are dissolved in the LC film and become deposited on the substrate surface during exposure to gaseous DMMP. Thus, 5CB cannot fully achieve its initial homeotropic alignment resulting in final correlation coefficients being less than $\rho = 1$.

As illustrated in Fig. 1, we replaced the rough diffuser with an analyzer having a polarization axis perpendicular to that of the first polarizer and mounted an imaging lens on the CCD camera to capture luminosity changes of the LC film. As shown by point A at $t = 0$ s in Fig. 4

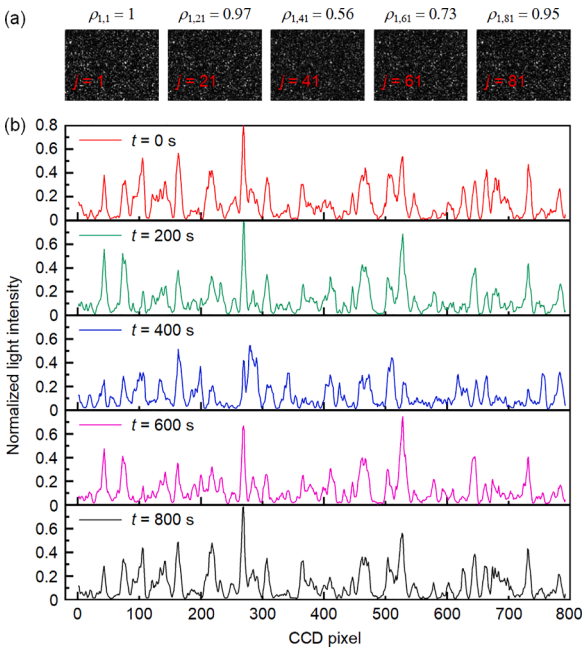

Fig. 5. Speckle images and correlation coefficients at separate times and light intensity distributions on each CCD pixel obtained from the 271st row of multiple speckle images. Speckle images were taken at 10-s intervals. (a) The 1st, 21st, 41st, 61st, and 81st speckle images and their correlation coefficients calculated relative to the 1st speckle image. (b) Light intensity distributions for all 792 CCD column pixels created by selecting the 271st row of the speckle images at $t = 0$ s (first row), $t = 200$ s (second row), $t = 400$ s (third row), $t = 600$ s (fourth row), and $t = 800$ s (fifth row).

(a), $\rho = 1$ and the initial appearance of the LC film is dark. At point B, which corresponds to exposure to 2 ppm DMMP vapor for 400 s, the correlation coefficient equals 0.56, and the optical appearance of the LC film is bright. After exposure of the LC film to pure nitrogen for 300 s (point C), ρ increases to 0.95, and the appearance of the LC film changes from bright to dark. The change in luminosity of the LC film induced by DMMP vapor is consistent with experimental phenomena observed in previous studies [15-19,24,34] and confirms that our method of characterizing the response and reversibility of LC films to DMMP vapor via changes of the speckle correlation coefficient is correct. Compared with traditional detection methods, such as those that use a polarizing optical microscope or a CCD camera with a mounted imaging lens to observe luminosity changes, our approach reduces the size and complexity of the experimental system. Detection results are also characterized more quantitatively via calculation of the correlation coefficient. Although the methodology reported adequately illustrates the sensitivity of the 5CB-Cu^{2+} LC films, we did not pursue an experimental system exhibiting maximum sensitivity and a lower DMMP detection limit, where the maximum sensitivity should be higher than 5 ppm because the correlation coefficients of the speckle images are not zero for 5 ppm DMMP. Figure 4(b) shows the responses of three sensors exposed to DMMP vapor for 500 s. The sensors show an acceptable repeatability with a maximum correlation coefficient variation from 0.66 to 0.54 for the 2 ppm DMMP vapor. This inconsistency may be caused by the LC film thickness differences of the sensors by filling LC into the TEM grids manually. This inconsistency can be minimized by using more advanced sensor fabrication techniques, for example, determining the LC film thickness by fabricating microwells or micropillars instead of using TEM grids [21,35].

We also examined speckle images of the LC sensor exposed to 2 ppm DMMP. The sensor was placed in the detection chamber and subjected to 2 ppm DMMP vapor for 500 s. The DMMP stream was stopped, and a flow of pure nitrogen was directed into the chamber for 300 s. Objective

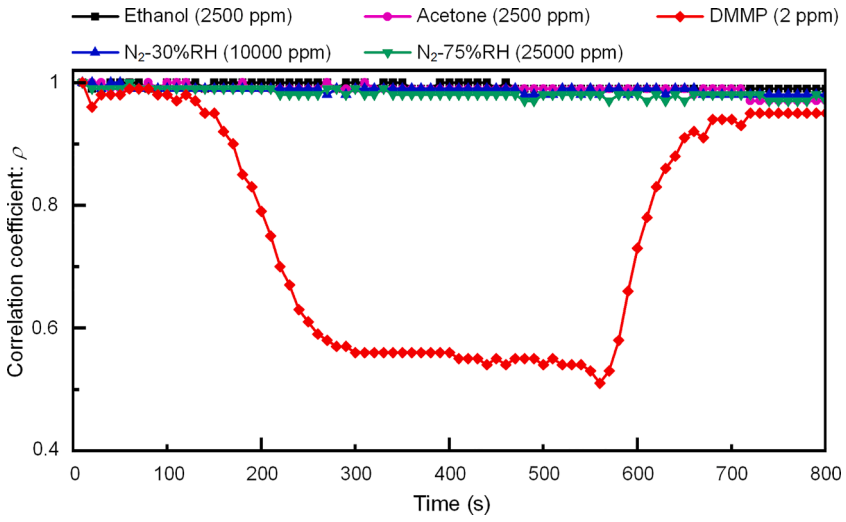

Fig. 6. Response of the 5CB-Cu^{2+} sensor to DMMP and several interfering vapors.

speckle images were captured by the CCD camera at 10 s. These experimental results show that the response of the LC sensor upon exposure to DMMP vapor and its reversibility following treatment with pure nitrogen are apparent from the changes in the speckle images (Fig. 5(a)) and light intensity distribution taken from the 271st row of pixels (Fig. 5(b)). These observations demonstrate the viability of characterizing the reversible and quantitative behavior of the liquid crystal DMMP sensor by capturing speckle images and calculating the correlation coefficient.

3.5. Gas sensor selectivity

We also exposed the supported 5CB-Cu^{2+} films to nitrogen streams containing different organic vapors and to streams at different relative humidity to investigate the selectivity of the sensor response. Figure 6 shows that the correlation coefficient does not decrease significantly upon exposing the LC film to 2500 ppm ethanol vapor and to 2500 ppm acetone vapor for 500 s. The LC film was exposed to a 26 °C nitrogen stream at 30% relative humidity (water vapor concentration ≈ 10,000 ppm) and 75% relative humidity (water vapor concentration ≈ 25,000 ppm) for 500 s [19]. The correlation coefficient does not decrease significantly under either condition. However, exposure of the same LC film to 2 ppm DMMP for 500 s causes ρ to decrease to 0.54. Figure 6 confirms that only DMMP initiates a reduction in the correlation coefficient and that the presence of H_2O or a common organic solvent does not displace the nitrile group of 5CB from its coordination with Cu^{2+} and drive an orientational transition within the LC film. We therefore conclude that the LC sensor selectivity responds to changes in the DMMP vapor content rather than changes in relative humidity or the presence of common organic solvents.

4. Conclusion

We developed a new method for determining the vapor phase concentration of DMMP based on the change in the correlation coefficient of laser speckles from a LC sensor. Compared with previous detection methods, neither a polarizing optical microscope nor a CCD camera with a mounted imaging lens and crossed polarizers is required. A rough diffuser is used to produce speckles, which reduces the size, complexity, and cost of the instrumentation. Our protocol also enables more quantitative detection results to be obtained by calculation of the correlation coefficients of speckle images. DMMP vapor is selectively detected over a 500 ppb to 5 ppm concentration range, although the sensitivity and detection limit of the sensor have not yet to be fully optimized. The LC sensor described in this work is based on 5CB, which has a narrow 22−35.1 °C nematic phase temperature range. We plan to investigate sensing devices based on different LCs, such as E7, to establish a greater range of operating temperatures. We will also consider introducing a smartphone to capture speckle images and further reduce the cost of the detection system. The results presented in this paper provide a useful template for the detection of vapor phase organophosphorus compounds using LC-based sensors.

CRediT authorship contribution statement

Yuxiang Yan: Conceptualization, Methodology, Software, Investigation, Data curation, Writing – original draft, Visualization. **Ning Bu:** Validation, Investigation. **Xiaoquan Bai:** Data curation. **Mei Wang:** Validation, Resources. **Yifei Ma:** Software, Formal analysis. **Suotang Jia:** Supervision, Funding acquisition. **Xuyuan Chen:** Supervision, Funding acquisition, Project administration. **Zhaomin Tong:** Conceptualization, Methodology, Validation, Writing – review & editing, Project administration, Funding acquisition.

Declaration of Competing Interest

The authors declare that they have no known competing financial interests or personal relationships that could have appeared to influence the work reported in this paper.

Data availability

Data will be made available on request.

Acknowledgments

This work was supported by the Key Research and Development Program of Shanxi Province (202102030201002); the Changjiang Scholars and Innovative Research Team in University of Ministry of Education of China (IRT_17R70); the State Key Program of National Natural Science of China (11434007); the 111 Project (D18001); the Fund for Shanxi "1331 Project" Key Subjects Construction.

References

[1] Goud KY, Sandhu SS, Teymourian H, et al. Textile-based wearable solid-contact flexible fluoride sensor: toward biodetection of G-type nerve agents. Biosens Bioelectron 2021;182:113172. https://doi.org/10.1016/j.bios.2021.113172.

[2] Leikin JB, Thomas RG, Walter FG, et al. A review of nerve agent exposure for the critical care physician. Crit Care Med 2002;30(10):2346–54. https://doi.org/10.1097/00003246-200210000-00026.
[3] Yanagisawa N, Morita H, Nakajima T. Sarin experiences in Japan: acute toxicity and long-term effects. J Neurol Sci 2006;249(1):76–85. https://doi.org/10.1016/j.jns.2006.06.007.
[4] Yang Z, Zhang Y, Gao S, et al. Hydrogen bonds-induced room-temperature detection of DMMP based on polypyrrole-reduced graphene oxide hybrids. Sens Actuators B Chem 2021;346:130518. https://doi.org/10.1016/j.snb.2021.130518.
[5] Easter RN, Caruso JA, Vonderheide AP. Recent developments and novel applications in GC-ICPMS. J Anal Atom Spectrom 2010;25(4):493–502. https://doi.org/10.1039/b924393n.
[6] Steiner WE, Klopsch SJ, English WA, et al. Detection of a chemical warfare agent simulant in various aerosol matrixes by ion mobility time-of-flight mass spectrometry. Anal Chem 2005;77(15):4792–9. https://doi.org/10.1021/ac050278f.
[7] Long Y, Wang Y, Du X, et al. The different sensitive behaviors of a hydrogen-bond acidic polymer-coated SAW sensor for chemical warfare agents and their simulants. Sensors 2015;15(8):18302–14. https://doi.org/10.3390/s150818302.
[8] Xu S, Zhang R, Cui J, et al. Surface acoustic wave DMMP gas sensor with a porous graphene/PVDF molecularly imprinted sensing membrane. Micromachines 2021;12(5):552. https://doi.org/10.3390/mi12050552.
[9] Li H, Zheng Q, Luo J, et al. Impacts of meso-structure and organic loadings of fluoroalcohol derivatives/SBA-15 hybrids on nerve agent simulant sensing. Sens Actuators B Chem 2013;187:604–10. https://doi.org/10.1016/j.snb.2013.04.122.
[10] Lee YJ, Kim JG, Kim JH, et al. Detection of dimethyl methylphosphonate (DMMP) using polyhedral oligomeric silsesquioxane (POSS). J Nanosci Nanotechnol 2018;18(9):6565–9. https://doi.org/10.1166/jnn.2018.15698.
[11] Thamri A, Baccar H, Struzzi C, et al. MHDA-functionalized multiwall carbon nanotubes for detecting non-aromatic VOCs. Sci Rep 2016;6(1):1–12. https://doi.org/10.1038/srep35130.
[12] Devi M, A K, Pani I, et al. Label-free detection of ochratoxin a using aptamer as recognition probe at liquid crystal-aqueous interface. Front Soft Matter 2022;2(1):835057. https://doi.org/10.1021/acs.langmuir.8b04018.
[13] Devi M, Pani I, Pal SK. Liquid crystals as signal transducers for sensing of analytes using aptamer as a recognition probe. Liq Cryst Rev 2022;9(2):65–84. https://doi.org/10.1080/21680396.2022.2053597.
[14] Verma I, Devi M, Sharma D, et al. Liquid crystal based detection of Pb (II) ions using Spinach RNA as recognition probe. Langmuir 2019;35(24):7816–23. https://doi.org/10.1021/acs.langmuir.8b04018.
[15] Sridharamurthy SS, Cadwell KD, Abbott NL, et al. A microstructure for the detection of vapor-phase analytes based on orientational transitions of liquid crystals. Smart Mater Struct 2007;17(1):012001. https://doi.org/10.1088/0964-1726/17/01/012001.
[16] Bungabong ML, Ong PB, Yang KL. Using copper perchlorate doped liquid crystals for the detection of organophosphonate vapor. Sens Actuators B Chem 2010;148(2):420–6. https://doi.org/10.1016/j.snb.2010.05.063.
[17] Yang KL, Cadwell K, Abbott NL. Use of self-assembled monolayers, metal ions and smectic liquid crystals to detect organophosphonates. Sens Actuators B Chem 2005;104(1):50–6. https://doi.org/10.1016/j.snb.2004.04.098.
[18] Cadwell KD, Lockwood NA, Nellis BA, et al. Detection of organophosphorous nerve agents using liquid crystals supported on chemically functionalized surfaces. Sens Actuators B Chem 2007;128(1):91–8. https://doi.org/10.1016/j.snb.2007.05.044.
[19] Roling LT, Scaranto J, Herron JA, et al. Towards first-principles molecular design of liquid crystal-based chemoresponsive systems. Nat Commun 2016;7(1):1–7. https://doi.org/10.1038/ncomms13338.
[20] Hunter JT, Pal SK, Abbott NL. Adsorbate-induced ordering transitions of nematic liquid crystals on surfaces decorated with aluminum perchlorate salts. ACS Appl Mater Interfaces 2010;2(7):1857–65. https://doi.org/10.1021/am100165a.
[21] Cheng D, Sridharamurthy SS, Hunter JT, et al. A sensing device using liquid crystal in a micropillar array supporting structure. J Microelectromech Syst 2009;18(5):973–82. https://doi.org/10.1109/JMEMS.2009.2029977.
[22] Chen D, Zhang K, Zhou H, et al. A wireless-electrodeless quartz crystal microbalance with dissipation DMMP sensor. Sens Actuators B Chem 2018;261:408–17. https://doi.org/10.1016/j.snb.2018.01.105.
[23] Emelianova A, Basharova EA, Kolesnikov AL, et al. Force fields for molecular modeling of Sarin and its simulants: DMMP and DIMP. J Phys Chem B 2021;125(16):4086–98. https://doi.org/10.1021/acs.jpcb.0c10505.
[24] Hunter JT, Abbott NL. Dynamics of the chemo-optical response of supported films of nematic liquid crystals. Sens Actuators B Chem 2013;183:71–80. https://doi.org/10.1016/j.snb.2013.03.094.
[25] Kim YK, Raghupathi KR, Pendery JS, et al. Oligomers as triggers for responsive liquid crystals. Langmuir 2018;34(34):10092–101. https://doi.org/10.1021/acs.langmuir.8b01944.
[26] Cadwell KD, Alf ME, Abbott NL. Infrared spectroscopy of competitive interactions between liquid crystals, metal salts, and dimethyl methylphosphonate at surfaces. J Phys Chem B 2006;110(51):26081–8. https://doi.org/10.1021/jp063211k.
[27] Dainty JC. Laser speckle and related phenomena, Vol. 9. Berlin, GER: Springer science & business Media; 2013.
[28] Goodman JW. Speckle phenomena in optics: theory and applications. Englewood. Colorado, USA: Roberts and Company Publishers; 2007.
[29] Tong Z, Chen X. Speckle contrast for superposed speckle patterns created by rotating the orientation of laser polarization. JOSA A 2012;29(10):2074–9. https://doi.org/10.1364/JOSAA.29.002074.
[30] Lu SY, Chipman RA. Mueller matrices and the degree of polarization. Opt Commun 1998;146(1–6):11–4. https://doi.org/10.1016/S0030-4018(97)00554-3.
[31] Polat Ö. Theoretical study on depolarization of the light transmitted through a non-uniform liquid crystal cell. Optik 2016;127(7):3560–3. https://doi.org/10.1016/j.ijleo.2015.12.166.
[32] Wei BY, Chen P, Ge SJ, et al. Liquid crystal depolarizer based on photoalignment technology. Photonics Res 2016;4(2):70–3. https://doi.org/10.1364/PRJ.4.000070.
[33] He S, Liang W, Cheng KL, et al. Bile acid–surfactant interactions at the liquid crystal/aqueous interface. Soft Matter 2014;10(26):4609–14. https://doi.org/10.1039/c4sm00486h.
[34] VanTreeck HJ, Most DR, Grinwald BA, et al. Quantitative detection of a simulant of organophosphonate chemical warfare agents using liquid crystals. Sens Actuators B Chem 2011;158(1):104–10. https://doi.org/10.1016/j.snb.2011.05.049.
[35] Bedolla Pantoja MA, Abbott NL. Surface-controlled orientational transitions in elastically strained films of liquid crystal that are triggered by vapors of toluene. ACS Appl Mater Interfaces 2016;8(20):13114–22. https://doi.org/10.1021/acsami.6b02139.